Molecular and functional resemblance of differentiated cells derived from isogenic human iPSCs and SCNT-derived ESCs

Ming-Tao Zhao[a,b,c,1], Haodong Chen[a,b,c,1], Qing Liu[d,1], Ning-Yi Shao[a,b,c], Nazish Sayed[a,b,c], Hung-Ta Wo[a,b,c,e], Joe Z. Zhang[a,b,c], Sang-Ging Ong[a,b,c], Chun Liu[a,b,c], Youngkyun Kim[a,b,c], Huaxiao Yang[a,b,c], Tony Chour[a,b,c], Hong Ma[f,g], Nuria Marti Gutierrez[f,g], Ioannis Karakikes[a,h], Shoukhrat Mitalipov[f,g,2], Michael P. Snyder[d,2], and Joseph C. Wu[a,b,c,2]

[a]Stanford Cardiovascular Institute, Stanford University School of Medicine, Stanford, CA 94305; [b]Division of Cardiology, Department of Medicine, Stanford University School of Medicine, Stanford, CA 94305; [c]Institute of Stem Cell Biology and Regenerative Medicine, Stanford University School of Medicine, Stanford, CA 94305; [d]Department of Genetics, Stanford University School of Medicine, Stanford, CA 94305; [e]Division of Cardiology, Department of Internal Medicine, Chang Gung Memorial Hospital, Linkou, 33305, Taiwan; [f]Center for Embryonic Cell and Gene Therapy, Oregon Health & Science University, Portland, OR 97239; [g]Division of Reproductive and Developmental Sciences, Oregon National Primate Research Center, Oregon Health & Science University, Beaverton, OR 97006; and [h]Department of Cardiothoracic Surgery, Stanford University School of Medicine, Stanford, CA 94305

Edited by R. Michael Roberts, University of Missouri, Columbia, MO, and approved November 7, 2017 (received for review May 30, 2017)

Patient-specific pluripotent stem cells (PSCs) can be generated via nuclear reprogramming by transcription factors (i.e., induced pluripotent stem cells, iPSCs) or by somatic cell nuclear transfer (SCNT). However, abnormalities and preclinical application of differentiated cells generated by different reprogramming mechanisms have yet to be evaluated. Here we investigated the molecular and functional features, and drug response of cardiomyocytes (PSC-CMs) and endothelial cells (PSC-ECs) derived from genetically relevant sets of human iPSCs, SCNT-derived embryonic stem cells (nt-ESCs), as well as in vitro fertilization embryo-derived ESCs (IVF-ESCs). We found that differentiated cells derived from isogenic iPSCs and nt-ESCs showed comparable lineage gene expression, cellular heterogeneity, physiological properties, and metabolic functions. Genome-wide transcriptome and DNA methylome analysis indicated that iPSC derivatives (iPSC-CMs and iPSC-ECs) were more similar to isogenic nt-ESC counterparts than those derived from IVF-ESCs. Although iPSCs and nt-ESCs shared the same nuclear DNA and yet carried different sources of mitochondrial DNA, CMs derived from iPSC and nt-ESCs could both recapitulate doxorubicin-induced cardiotoxicity and exhibited insignificant differences on reactive oxygen species generation in response to stress condition. We conclude that molecular and functional characteristics of differentiated cells from human PSCs are primarily attributed to the genetic compositions rather than the reprogramming mechanisms (SCNT vs. iPSCs). Therefore, human iPSCs can replace nt-ESCs as alternatives for generating patient-specific differentiated cells for disease modeling and preclinical drug testing.

somatic cell nuclear transfer | in vitro fertilization | embryonic stem cells | induced pluripotent stem cells | cardiomyocytes

The genome of a cell contains essential information to direct the entire development of a human body. During embryonic development, the genome can be transcribed to differential messenger RNAs in a cell-type–specific manner to establish diverse populations of stem cells, progenitor cells, and differentiated cells in the body. The lineage commitment is precisely regulated in a spatiotemporal manner but generally unidirectional in vivo. However, somatic cell lineage can be reverted back to the pluripotent state in vitro by nuclear reprogramming, which has been achieved by multiple approaches such as somatic cell nuclear transfer (SCNT), ectopic expression of transcription factors for reprogramming (induced pluripotent stem cells, iPSCs), and cell fusion (1). The SCNT method utilizes the cytoplasm of an unfertilized egg to reprogram the genome of a somatic cell into a totipotent state, which is the most complete and stringent epigenetic reprogramming process (2). SCNT-derived embryos can produce live cloned offspring if transferred to the uterus of a surrogate mother (i.e., reproductive cloning). Alternatively, embryonic stem cells (ESCs) can be derived from SCNT embryos (i.e., therapeutic cloning) (3). In contrast, iPSC reprogramming resets a somatic cell to a pluripotent state by transient overexpression of four transcription factors without using human eggs.

Human ESCs derived from in vitro fertilization (IVF) embryos have been considered the "gold standard" of pluripotent stem cells (4). Mammalian iPSCs are thought to be similar to the IVF-ESCs with respect to self-renewal and pluripotent lineage differentiation capacity (5). However, early-passage human iPSCs carry aberrant epigenetic memory of their parental somatic cells (6, 7). Whole-genome DNA methylation studies have identified memory-specific differentially methylated regions (DMRs) in human iPSCs compared with IVF-ESCs, including large-scale

Significance

Patient-specific pluripotent stem cells (PSCs) can be derived by two nuclear reprogramming methods: somatic cell nuclear transfer (SCNT) using unfertilized eggs and transcription factor-based reprogramming (i.e., induced pluripotent stem cells, iPSCs). The direct comparison of differentiated cells generated by SCNT and iPSC has yet to be assessed. In this study, we employ cutting-edge technologies to evaluate the similarities and differences between isogenic human iPSCs and SCNT-ESC derivatives. We provide proof-of-concept that differentiated cells derived from human iPSCs are comparable to nuclear transfer-derived ESC counterparts with regard to transcriptional, epigenetic, physiological, and pharmacological features, given that they are genetically identical. We conclude that human iPSCs are capable of replacing SCNT for generating differentiated cells for drug testing and disease modeling.

Author contributions: M.-T.Z., H.C., S.M., M.P.S., and J.C.W. designed research; M.-T.Z., H.C., Q.L., N.-Y.S., N.S., H.-T.W., J.Z.Z., S.-G.O., C.L., Y.K., H.Y., T.C., H.M., N.M.G., and I.K. performed research; M.-T.Z., H.C., Q.L., N.-Y.S., N.S., H.-T.W., J.Z.Z., S.-G.O., C.L., and Y.K. analyzed data; and M.-T.Z., H.C., Q.L., N.-Y.S., N.S., H.-T.W., J.Z.Z., S.-G.O., H.Y., T.C., H.M., N.M.G., I.K., S.M., M.P.S., and J.C.W. wrote the paper.

The authors declare no conflict of interest.

This article is a PNAS Direct Submission.

Data deposition: The data reported in this paper have been deposited in the Gene Expression Omnibus (GEO) database, https://www.ncbi.nlm.nih.gov/geo (accession no. GSE94267).

[1]M.-T.Z., H.C., and Q.L. contributed equally to this work.

[2]To whom correspondence may be addressed. Email: mitalipo@ohsu.edu, mpsnyder@stanford.edu, or joewu@stanford.edu.

This article contains supporting information online at www.pnas.org/lookup/suppl/doi:10.1073/pnas.1708991114/-/DCSupplemental.

aberrant non-CG methylation regions close to centromeres and telomeres (8). Although isogenic nuclear transfer-derived ESCs (nt-ESCs) and iPSCs display comparable numbers of de novo copy number variations and frequency of coding region mutations (9), nt-ESCs are considered to be free of somatic epigenetic memory and are more similar to conventional IVF-ESCs in their transcriptomic and epigenomic signatures (10, 11).

Human iPSCs and nt-ESCs can be derived in a patient- and disease-specific manner, potentially transforming the fields of modeling genetically inherited diseases and novel drug discovery (12). The terminally differentiated cells, such as cardiomyocytes (CMs) and endothelial cells (ECs), are the most suited for personalized medicine because they are the end-stage cells for cell transplantation therapy and high-throughput drug screening (13). In this study, we generated genetically relevant sets of human iPSCs, nt-ESCs, and IVF-ESCs. Human iPSCs and nt-ESCs were derived from the same donor cells, thus sharing the same nuclear DNA but different mitochondrial DNA. IVF-ESCs were generated using the oocytes from the same egg donor for SCNT and carried the same mitochondrial DNA with nt-ESCs due to the maternal inheritance of mitochondria. We evaluated the molecular and functional behaviors, and drug response of terminally differentiated cells derived from these PSCs created by different reprogramming mechanisms. We provide proof-of-concept that terminally differentiated cells derived from isogenic human nt-ESCs and iPSCs are relatively equivalent with respect to transcriptional, epigenomic, and functional features.

Results

Generation of Genetically Relevant Sets of Human iPSCs, nt-ESCs, and IVF-ESCs. The overall experimental design is depicted in Fig. 1*A*. Human iPSCs were generated from dermal fibroblasts via Sendai virus-based vectors. The isogenic nt-ESCs were derived from cloned embryos that were created by injecting the dermal fibroblasts from the same individuals to enucleated eggs (14). Human IVF-ESCs were generated following in vitro fertilization of oocytes from the same egg donor used for SCNT. Thus, human iPSCs and nt-ESCs were isogenic, whereas nt-ESCs and IVF-ESCs were genetically relevant because they shared the same mitochondria inherited from the same egg donor. In total, four human PSC clones were generated from two individuals (two clones for each person) for each reprogramming method (iPSCs, nt-ESCs, and IVF-ESCs). These PSCs formed typical stem cell colonies and were morphologically indistinguishable among each other (Fig. S1*A*). Similarly, these PSCs expressed the pluripotency markers OCT3/4 and NANOG (Fig. S1*B*). The majority of cells in

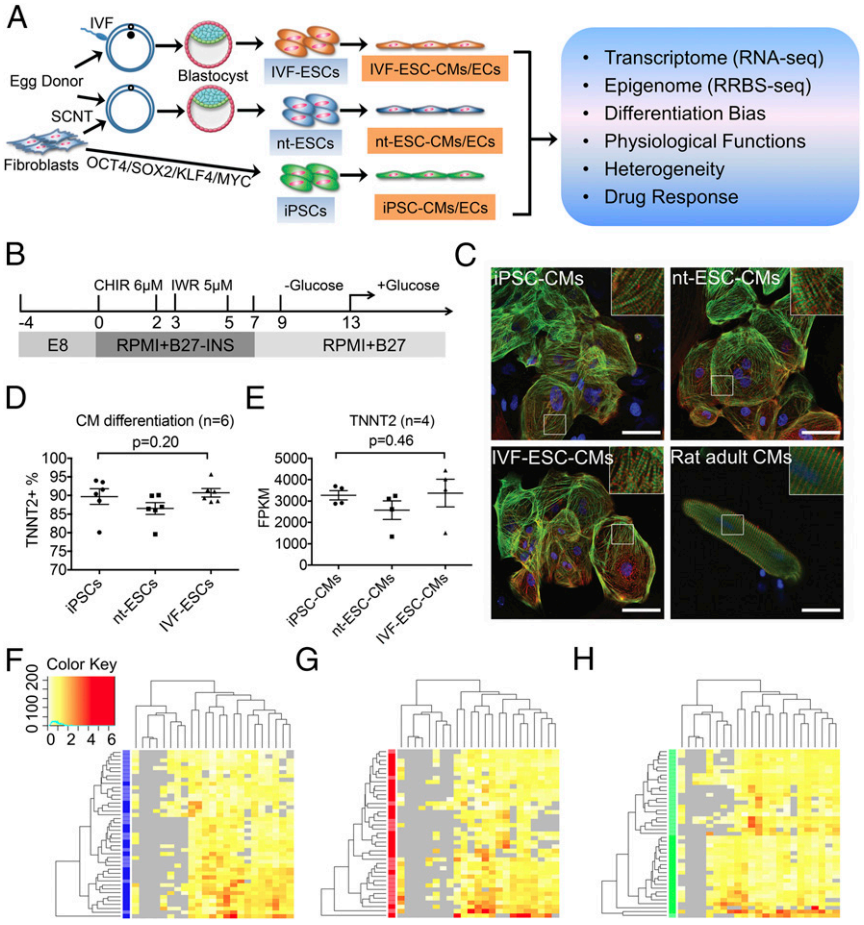

Fig. 1. Cardiac differentiation of genetically relevant sets of human iPSCs, nt-ESCs, and IVF-ESCs. (*A*) Overview of experimental design in this study. (*B*) A small-molecule–mediated monolayer cardiac differentiation protocol. (*C*) Cardiac troponin T (green) and α-actinin (red) double staining illustrated the sarcomere structures of PSC-CMs and rat adult CMs. The nuclei were counterstained by DAPI (blue). (Scale bars, 25 μm.) (Original magnifications: 600×.) (*D*) Cardiac differentiation efficiency calculated by the percentage of $TNNT2^+$ cells using flow cytometry. (*E*) Cardiac TNNT2 expression in iPSC-CMs, nt-ESC–CMs, and IVF-ESC-CMs. (*F–H*) Single-cell qPCR analysis of heterogeneity in CMs derived from different sources of PSCs. Blue: iPSC-CMs (*F*); red: nt-ESC-CMs (*G*); green: IVF-ESC-CMs (*H*). Heavy and light colors indicate two cell lines in each PSC-CM category. Each row represents a single cell, whereas each column indicates a single gene. The color key applies to *F–H*. *P* values were determined by one-way ANOVA. Error bars indicate SEM.

the colonies were pluripotent, as evidenced by high percentages of $OCT4^+/NANOG^+$ and $SSEA4^+/TRA\text{-}1\text{-}60^+$ (Fig. S1 *C* and *D*) cells in the population. The mitochondrial DNA genotyping was carried out to confirm the identity of these PSCs. As shown in Fig. S1*E*, two mitochondrial SNP sites (16187 A/C and 16193 T/C) were used. The mitochondrial DNA of iPSCs was inherited from somatic cells, thus carrying C (16187) and C (16193) after Sanger sequencing. In contrast, mitochondria of nt-ESCs and IVF-ESCs were derived from the donor oocytes and reflected as A (16187) and T (16193) (Fig. S1*F*), because mitochondrial DNA is maternally inherited during early embryonic development. We also tested these SNP sites in differentiated PSC-CMs and PSC-ECs and confirmed their cellular identity after terminal differentiation.

Cardiac Differentiation of Human iPSCs, nt-ESCs, and IVF-ESCs. To explore the similarities and differences in differentiated cells derived from iPSCs, nt-ESCs, and IVF-ESCs, we differentiated them into CMs using a small-molecule–mediated differentiation protocol (Fig. 1*B*). Upon differentiation, human iPSCs, nt-ESCs, and IVF-ESCs all formed a sheet-like structure that could beat synchronously for a long time (>2 months). Close examination by immunofluorescence staining showed cardiac sarcomere structures with intercalating cardiac troponin T (TNNT2) and α-actinin distribution in all PSC-CMs, which were morphologically different from the rod-shaped adult rat CMs (Fig. 1*C*). Cardiac differentiation efficiency was not significantly different among iPSCs, nt-ESCs, and IVF-ESCs (Fig. 1*D*). In addition, cardiac differentiation efficiency variance among clones from the same reprogramming mechanism was not statistically significant (Fig. S1 *G–I*). Similarly, the expression of cardiac structure genes *TNNT2* (Fig. 1*E*) and *MYH7* (Fig. S1*J*) was similar among these PSC-CMs. We then tested whether the proportion of the CM subtypes (atrial and ventricular) was differentially represented. We surveyed the gene expression of atrial markers (*MYL7*: myosin light chain 7, regulatory; and *NPPA*: atrial natriuretic peptide) and ventricular markers (*MYL2*: myosin light chain 2, regulatory; and *NPPB*: ventricular natriuretic peptide) among these PSC-CMs. We did not observe any skewed cardiac differentiation toward either atrial or ventricular subtypes between iPSC-CMs and nt-ESC–CMs (Fig. S1 *K–N*). Furthermore, the ability of intercellular communication and ion transportation of PSC-CMs seems to be commensurate as *GJA1* (gap junction α-1), potassium channel gene *KCNQ1*, and calcium channel gene *CACNA1C* were not differentially expressed among iPSC-CMs, nt-ESC–CMs, and IVF-ESC-CMs (Fig. S1 *O–Q*).

Next, we evaluated the gene expression heterogeneity of iPSC-CMs, nt-ESC–CMs, and IVF-ESC-CMs using microfluidic single-cell qPCR. We selected a panel of genes associated with different cardiac functions (Table S1), including cardiac development (*KDR*, *MEF2C*, *ISL1*, and *TBX5*), cardiac structure (*TNNT2* and *MYH7*), atrial (*NPPA*) and ventricular (*NPPB*) markers, nodal cells (*TBX18*), gap junction (*GJA1* and *GJA5*), ion channels (*KCNH2*, *SCN5A*, and *CACNA1C*), and vascular endothelial lineage (*CD31* and *CD144*). Single iPSC-CMs shared similar gene-expression profiles with nt-ESC–CMs, such as highly expressed CM genes and lowly expressed cardiac progenitor and endothelial genes (Fig. 1 *F–H*). Hierarchical clustering of single-cell gene expression displayed a similar heterogeneity pattern between iPSC-CMs (Fig. 1*F*) and nt-ESC–CMs (Fig. 1*G*). Overall, these data suggest that the gene-expression heterogeneity is comparable among CMs derived from human iPSCs and isogenic nt-ESCs.

We then assessed the physiological and metabolic features of iPSC-CMs, nt-ESC–CMs, and IVF-ESC-CMs. We compared the myocardial contraction ability of these PSC-CMs, including beating rate, contraction velocity, relaxation velocity, and acceleration. Sheets of PSC-CMs derived from different reprogramming mechanisms were beating with synchronized rhythm in the field and did not show significant difference in these contraction and relaxation parameters (Fig. S2 *A–D* and Movies S1–S3). Because calcium (Ca^{2+}) is a critical regulator of cardiac myocyte function and mediates excitation–contraction coupling (15), we next evaluated the Ca^{2+} handling capability among these PSC-CMs. We did not observe any significant difference in the Ca^{2+} flux during excitation–contraction coupling, including the diastolic Ca^{2+}, time to peak, and half decay time between iPSC-CMs, nt-ESC–CMs, and IVF-ESC-CMs (Fig. S2 *E–H*), suggesting they have comparable Ca^{2+} handling capacity. Because these PSC-CMs shared distinct combinations of nuclear genome and mitochondrial DNA (iPSC-CMs and nt-ESC–CMs had the same nuclear genome but different mitochondrial DNA, whereas nt-ESC–CMs and IVF-ESC–CMs shared the same mitochondria but different nuclear genomes), we further evaluated the mitochondrial function by a Seahorse assay. At both basal and maximal respiration levels, these PSC-CMs did not show significant differences at oxygen consumption rate across multiple time points (Fig. S2 *I–K*). The ATP production and spare respiration capacity were nearly the same for these PSC-CMs (Fig. S2*L*). Taken together, these data suggest that the isogenic iPSC-CMs and nt-ESC–CMs exhibit negligible functional difference at the electrophysiological and metabolic levels, irrespective of the divergent sources of mitochondria.

Endothelial Differentiation of Human iPSCs and nt-ESCs, and IVF-ESCs. We next tested the endothelial differentiation capacity of these three types of human PSCs by a monolayer differentiation protocol (Fig. 2*A*). All of these PSC-ECs showed similar endothelial differentiation and maintenance efficiencies (Fig. 2 *B* and *D*), suggesting that reprogramming methods (iPSC or SCNT) do not affect endothelial differentiation. In addition, we did not observe any significant difference in endothelial differentiation efficiency among clones derived from the same reprograming method (Fig. S3 *A–C*). We then explored the functional similarities and differences of ECs derived from iPSCs, nt-ESCs, and IVF-ESCs. These PSC-ECs expressed the endothelial surface markers CD31, CD144 (Fig. 2*C*), and von Willebrand factor (vWF), and took up low-density lipoprotein (LDL) (Fig. S3 *D* and *E*). The expression of endothelial marker genes *PECAM1* and *CDH5* was not statistically different among these PSC-ECs (Fig. 2 *E* and *F*). Similarly, *NOS3* mRNA was expressed at comparable levels among iPSC-ECs, nt-ESC–ECs, and IVF-ESC-ECs (Fig. 2*G*). Next we evaluated the capacity of these PSC-ECs to produce nitric oxide and found no significant difference among them (Fig. 2*H*). Furthermore, these PSC-ECs formed tube-like structures when placed on Matrigel (Fig. S3*F*). The branches of tubes were not statistically different among iPSC-ECs, nt-ESC–ECs, and IVF-ESC-ECs, indicating similar in vitro angiogenesis ability (Fig. 2*I*).

As endothelial cells form blood vessels consisting of venous, arterial, and lymphatic subtypes, we tested whether there was a bias of specific subtypes to which PSC-ECs tended to differentiate. We assessed the mRNA abundance of markers for venous (*EPHB4*), arterial (*EFNB2*, *NOTCH1*, and *NOTCH4*), and lymphatic (*LYVE1* and *PROX1*) subtypes. The venous and arterial markers (Fig. S3 *G–J*) were not significantly different among iPSC-ECs, nt-ESC–ECs, and IVF-ESC-ECs, indicating that there is no biased differentiation toward arterial and venous subtypes. For the lymphatic markers, *LYVE1* maintained a significantly higher level in IVF-ESC-ECs, whereas *PROX1* was expressed at similar levels among these PSC-ECs (Fig. S3 *K* and *L*). Taking these data together, we found that iPSC-ECs and isogenic nt-ESC–ECs exhibited comparable features in endothelial marker gene expression, endothelial differentiation efficiency, NO production, in vitro angiogenesis, and endothelial subtypes.

Transcriptional Comparisons of CMs and ECs Derived from Human iPSCs, nt-ESCs, and IVF-ESCs. Gene expression is considered the key determinant of cellular phenotype, and transcriptional variations underlie the individual phenotypes in a given cell type (16).

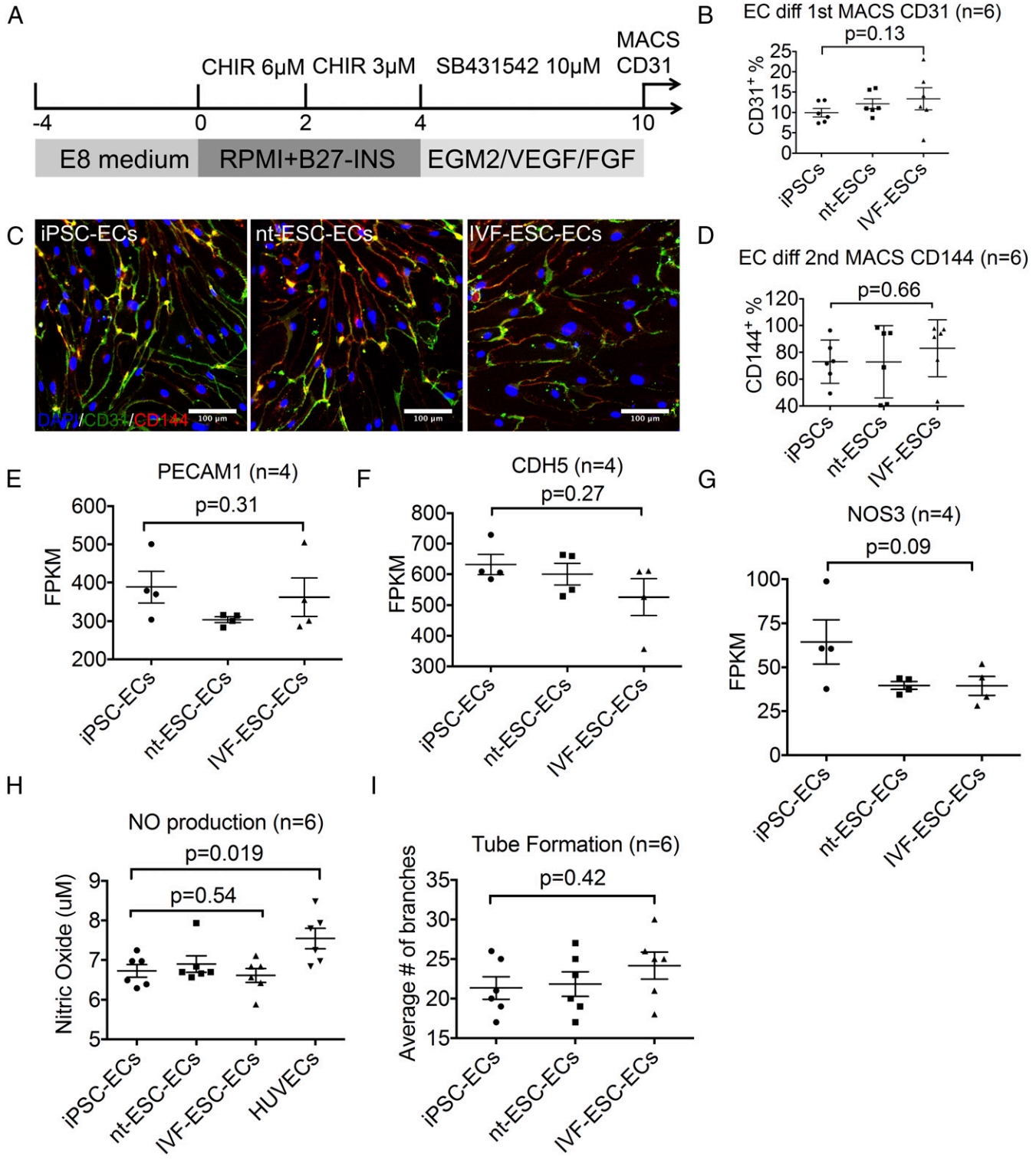

Fig. 2. ECs derived from multiple sources of PSCs. (*A*) Small-molecule–mediated endothelial differentiation protocol. (*B*) Endothelial differentiation efficiency evaluated by the percentage of $CD31^+$ cells at D12 of differentiation. (*C*) Representative immunofluorescence staining of PSC-ECs using CD31 and CD144 monoclonal antibodies. The nuclei were counterstained with DAPI. (Scale bars, 100 μm.) (*D*) Endothelial maintenance was assessed by the percentage of $CD144^+$ cells. No significant differences were observed among iPSC-ECs, nt-ESC–ECs, and IVF-ESC-ECs. (*E*–*G*) EC-specific marker genes (*E*) *PECAM1*, (*F*) *CDH5*, and (*G*) *NOS3* were expressed at similar levels in iPSC-ECs, nt-ESC–ECs, and IVF-ESC-ECs. (*H*) Nitric oxide production in PSC-ECs and human umbilical vein endothelial cells (HUVECs). (*I*) Average number of branches in the tubes formed by PSC-ECs. Data are presented as mean ± SEM. *P* values were calculated using one-way ANOVA.

To further pinpoint the gene-expression profiles of terminally differentiated cells derived from iPSCs, nt-ESCs, and IVF-ESCs, we performed whole-transcriptome analysis using high-throughput RNA sequencing (n = 36). We used unsupervised hierarchical clustering to view the distance among iPSCs, nt-ESCs, and IVF-ESCs in an undifferentiated state. The transcriptional program of

iPSCs was clustered closer to nt-ESCs than to IVF-ESCs (Fig. S4*A*). We then carried out hierarchical clustering of all PSCs, PSC-CMs, and PSC-ECs together based on differentially expressed genes (DEGs). Apparently, cell type-specific transcriptional programs were dominant, with the majority of variance stemming from the difference between distinct cell types (i.e., PSCs, CMs, and ECs). A principal component analysis (PCA) plot delineated the separation of PSCs, PSC-CMs, and PSC-ECs at the whole-transcriptome level (Fig. S4*C*). Unsupervised hierarchical clustering analysis showed consistently closer transcriptional profiles between iPSCs and isogenic nt-ESCs compared with IVF-ESCs in both undifferentiated and differentiated cells (Fig. 3*A*), suggesting that the transcriptional resemblance of isogeneic human iPSCs and nt-ESCs is well maintained regardless of differentiation status. Next we examined the DEGs among iPSCs, nt-ESCs, and IVF-ESCs before and after differentiation. There were 654 DEGs found among iPSCs, nt-ESCs, and IVF-ESCs (Fig. 3*C*), most of which were associated with antigen processing, presentation of peptide antigen, and MHC class II (Fig. S4*F*). We then asked whether the transcriptional similarity between iPSCs and nt-ESCs (compared with IVF-ESCs) could be inherited by terminally differentiated cells (CMs and ECs). We compared the transcriptional profiles of day 30 iPSC-CMs, nt-ESC–CMs, and IVF-ESC-CMs. In total, we identified 205 DEGs and hierarchical clustering showed that iPSC-CMs were clustered together with nt-ESC–CMs within the same clade, but were separated from IVF-ESC-CMs (Fig. S4*B*), suggesting that the transcriptional similarity between iPSCs and nt-ESCs is inheritable during cellular differentiation. Gene ontology (GO) analysis showed that antigen processing and presentation, lipid and fatty acid biosynthetic processes, and response to DNA damage stimulus were significantly enriched (Fig. 3*D*).

We next evaluated the transcriptional resemblance of PSC-ECs. We identified 507 DEGs among iPSC-ECs, nt-ESC–ECs, and IVF-ESC-ECs (Fig. 3*C*). Hierarchical clustering of PSC-ECs placed iPSC-ECs in the same clade with nt-ESC–ECs, but separate from IVF-ESC-ECs (Fig. 3*B*). In addition, these DEGs were related to the regulation of transcription, RNA metabolic

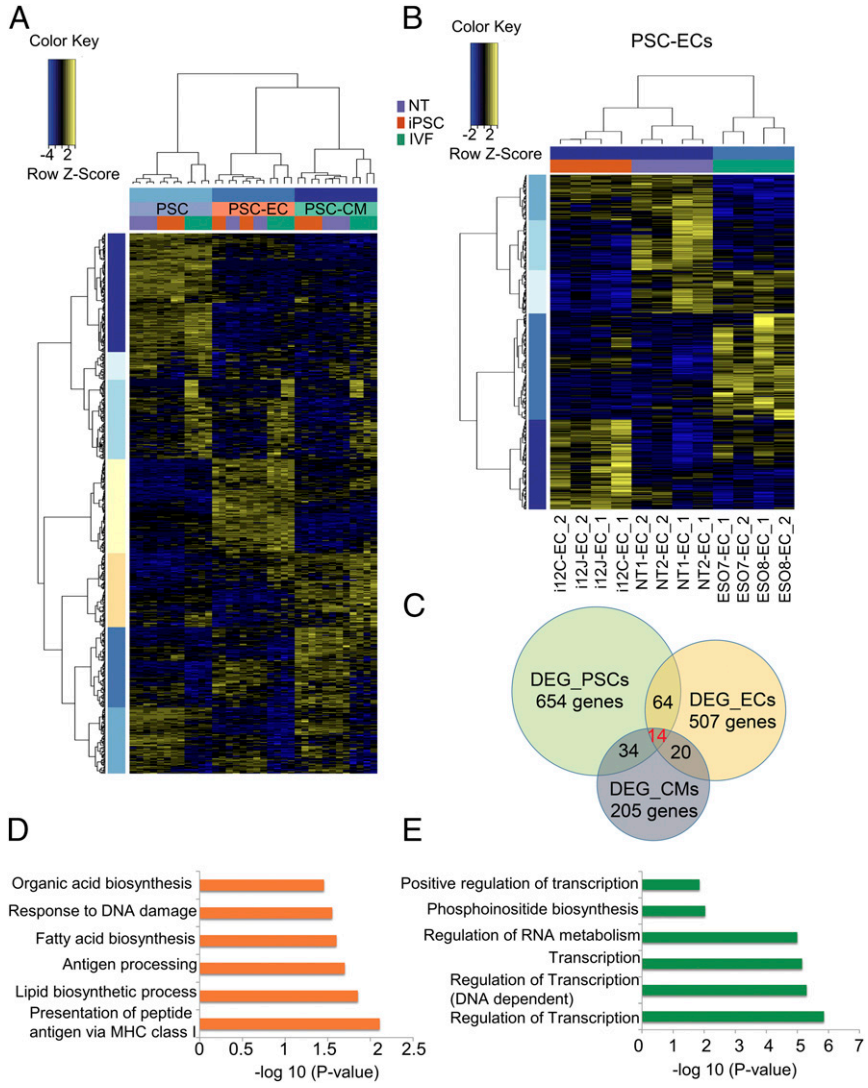

Fig. 3. Global gene-expression profiles of PSCs, PSC-CMs, and PSC-ECs revealed by RNA-seq. (*A*) Unsupervised hierarchical clustering of DEGs between PSCs, PSC-CMs, and PSC-ECs ($q < 0.1$). (*B*) PSC-ECs were clustered together based on reprogramming approaches used for generating iPSCs (i12C, i12J), nt-ESCs (NT1, NT2), and IVF-ESCs (ESO7, ESO8) ($q < 0.1$). (*C*) Numbers of DEGs identified in PSCs, PSC-CMs, and PSC-ECs due to reprogramming approaches. Overlapping regions represent the number of consistent DEGs. (*D*) GO analysis of DEGs among iPSC-CMs, nt-ESC-CMs, and IVF-ESC-CMs ($P < 0.05$). (*E*) GO terms of DEGs in ECs derived from iPSCs, nt-ESCs, and IVF-ESCs ($P < 0.05$).

process, and phosphoinositide biosynthetic process (Fig. 3*E*). Taken together, these data suggest that immunological process drives the major differences in undifferentiated state, whereas metabolic activities and transcriptional regulation account for the major differences among iPSCs, nt-ESCs, and IVF-ESCs after terminal differentiation.

We further explored the conserved DEGs before and after differentiation. We found 14 genes (Table S2) overlapped in PSCs, PSC-CMs, and PSC-ECs, which were consistently differentially expressed among iPSCs, nt-ESCs, and IVF-ESCs, and maintained the differential expression in terminally differentiated cells (PSC-CMs and PSC-ECs). As examples, *NAPRT* (nicotinate phosphoribosyltransferase) was significantly up-regulated in IVF-ESCs than iPSCs and nt-ESCs, whereas *FIS1* (mitochondrial fission 1) was down-regulated in IVF-ESCs compared with iPSCs and nt-ESCs (Fig. S4 *D* and *E*). NAPRT is a coenzyme in cellular redox reactions that converts nicotinic acid to nicotinamide adenine dinucleotide, with a role in a variety of cellular metabolic processes in response to stress conditions (17). FIS1 is a component of a mitochondrial complex that promotes mitochondrial fission and helps regulate mitochondrial morphology, cell cycle, and apoptosis (18). The consistent differential expression of *NAPRT* and *FIS1* may imply a fundamental difference in energy metabolism among different types of PSCs, which is likely due to a differential combination of genomic and mitochondrial DNAs resulting from distinct nuclear reprogramming mechanisms (iPSC, SCNT, and IVF). In addition, when these common DEGs were clustered together, iPSCs and nt-ESCs and their differentiated cells (CMs and ECs) displayed distinguishable gene-expression profiles from those of IVF-ESCs (Fig. S4*G*). Taken together, these results indicate that terminally differentiated cells derived from iPSCs are comparable to those from isogenic nt-ESCs, but are distinguishable from IVF-ESC derivatives at the transcriptional level.

Because clone-to-clone transcriptional variance may be a confounding factor for lineage differentiation (19), we then looked into the correlation of gene expression between clones derived from the same reprogramming mechanism in undifferentiated (PSC) and differentiated cells (PSC-ECs and PSC-CMs). We found transcriptional variance among clones from the same reprogramming mechanism was smaller than that from different reprogramming mechanisms using unsupervised hierarchical clustering. Clones from different reprogramming methods were clustered in a higher clade than those from the same reprogramming method, indicating larger transcriptional dissimilarity exists in clones derived from different reprogramming methods (Fig. S5*A*). PCA also pointed out that the clone-to-clone variance was much smaller than that introduced by reprogrammed methods (Fig. S5 *B* and *C*). In fact, correlation of gene expression between clones was very high in both undifferentiated PSCs and differentiated cells (PSC-CMs and PSC-ECs) (Fig. S6). Taken together, these results suggest that gene expression variance caused by the reprogramming methods (iPSC, SCNT, and IVF) is much larger than that contributed by the clone-to-clone difference.

Genome-Wide DNA Methylation Profiles of PSCs and Differentiated Cells. DNA methylation conveys stable epigenetic marks to establish the cellular identity and maintain epigenetic memory during cellular reprogramming and differentiation (20). To examine DNA methylome reprogramming during lineage commitment in these PSCs, we next performed genome-wide high-throughput reduced-representation bisulfite sequencing (RRBS-seq) (n = 18). We found that CG methylation was prevalent across PSCs, PSC-CMs, and PSC-ECs, whereas non-CG methylation constituted less than 15% of all methylated cytosines (Fig. 4*A*). After terminal differentiation, non-CG methylation (primarily mCHG) decreased in PSC-CMs and PSC-ECs (Fig. S7*A*). Overall, we did not observe any significant difference in the percentages of global mCG, mCHG, and mCHH among these PSCs and their respective CMs and ECs. Furthermore, all PSCs, PSC-CMs, and PSC-ECs exhibited genome-wide bimodal CG methylation patterns: most of the CpG sites were either highly methylated (>80%) or unmethylated (<20%) (Fig. S7 *B* and *C*). The bimodal DNA methylation distribution was conserved in mammalian PSCs and differentiated cells (21).

Next, we compared the epigenetic similarity by unsupervised hierarchical clustering of the genome-wide CG methylation. At the undifferentiated stage, iPSCs and nt-ESCs were clustered together in the same clade but were separated from IVF-ESCs (Fig. 4*B*). After induced differentiation, CMs and ECs derived from iPSCs and nt-ESCs were still clustered more closely than those derived from IVF-ESCs, suggesting that the epigenetic resemblance between iPSCs and nt-ESCs was well retained in differentiated cells. Within each condition (undifferentiated and differentiated), the overall correlation coefficient among PSCs was high (Fig. S7 *D*–*F*). We then carried out pairwise comparisons to locate differentially methylated cytosines (DMCs) at single CpG sites. In undifferentiated PSCs, we identified 48,203 DMCs between IVF-ESCs and nt-ESCs, and 52,344 DMCs between IVF-ESCs and iPSC (Fig. 4*C*). However, there were only 15,853 DMCs between nt-ESCs and iPSCs. Similarly, the difference in the number of DMCs between nt-ESC–CMs and iPSC-CMs was the smallest (12,489) among the pairwise comparisons. In addition, nt-ESC–ECs and iPSC-ECs were separated by 24,300 DMCs, ranking the lowest among the possible pairwise combinations (Fig. 4*C*). Overall, nt-ESCs vs. iPSCs had the lowest number of DMCs, whereas IVF-ESCs versus iPSCs held the largest number of DMCs, regardless of differentiation status.

CpG islands (CGIs) are short-interspersed DNA sequences containing a higher CG frequency than other regions in the genome, whereas CGI shores (up to 2 kb away) are the immediate regions flanking CGIs (22). Because CGIs are predominantly located at transcription start sites, CGI methylation is often associated with transcriptional silencing (23). In the present study, we identified DMRs of CGIs and CGI shores in PSCs, PSC-CMs, and PSC-ECs. For CGIs, we located 3,452 DMRs (from a total of 21,341 CGIs) between PSCs, PSC-CMs, and PSC-ECs (Fig. 4*D*). For CGI shores (2-kb flanking CGIs), we found 2,324 DMRs (from a total of 31,530 CGI shores) between PSCs, PSC-CMs, and PSC-ECs (Fig. 4*E*). Unsupervised hierarchical clustering of DMRs in CGIs and CGI shores consistently positioned iPSCs and nt-ESCs within the same clades, but both were distinguishable from IVF-ESCs in both undifferentiated and differentiated states.

We further looked into the DMRs that were consistently present in PSCs, PSC-CMs, and PSC-ECs. We also included DMRs in promoter regions (1-kb flanking transcription start sites) since DNA methylation in promoter regions is often associated with gene regulation. To remove the contributing factor of cell types (PSC, PSC-CMs, and PSC-ECs), we recalled DMRs within each cell type using the reprogramming method (iPSC, NT, or IVF) as a factor. For CGIs, there were 405 DMRs in PSCs, 468 DMRs in PSC-CMs, and 475 DMRs in PSC-ECs (Fig. S8*A*). We then examined the DMRs that were consistently retained in PSCs, PSC-CMs, and PSC-ECs. Interestingly, we found 42 consistent CGI DMRs, 40 consistent CGI shore DMRs, and 15 consistent promoter DMRs. Of these consistent DMRs, most of them (88) were IVF-specific, whereas only nine DMRs were iPSC-specific (Fig. S8*C*). Hierarchical clustering of consistent DMRs in CGIs, CGI shores, and promoters (Fig. 5 *A* and *B* and Fig. S8*B*) clearly divided these variables into three clades, depending on reprogramming methods. Furthermore, the majority of these consistent DMRs were between iPSCs and IVF-ESCs with no SCNT-specific DMRs found (Fig. 5*C* and Fig. S8*C*). A further look into the DNA methylation information showed that iPSCs and nt-ESCs shared similar DNA methylation levels compared with those in IVF-ESCs. This occurred in both

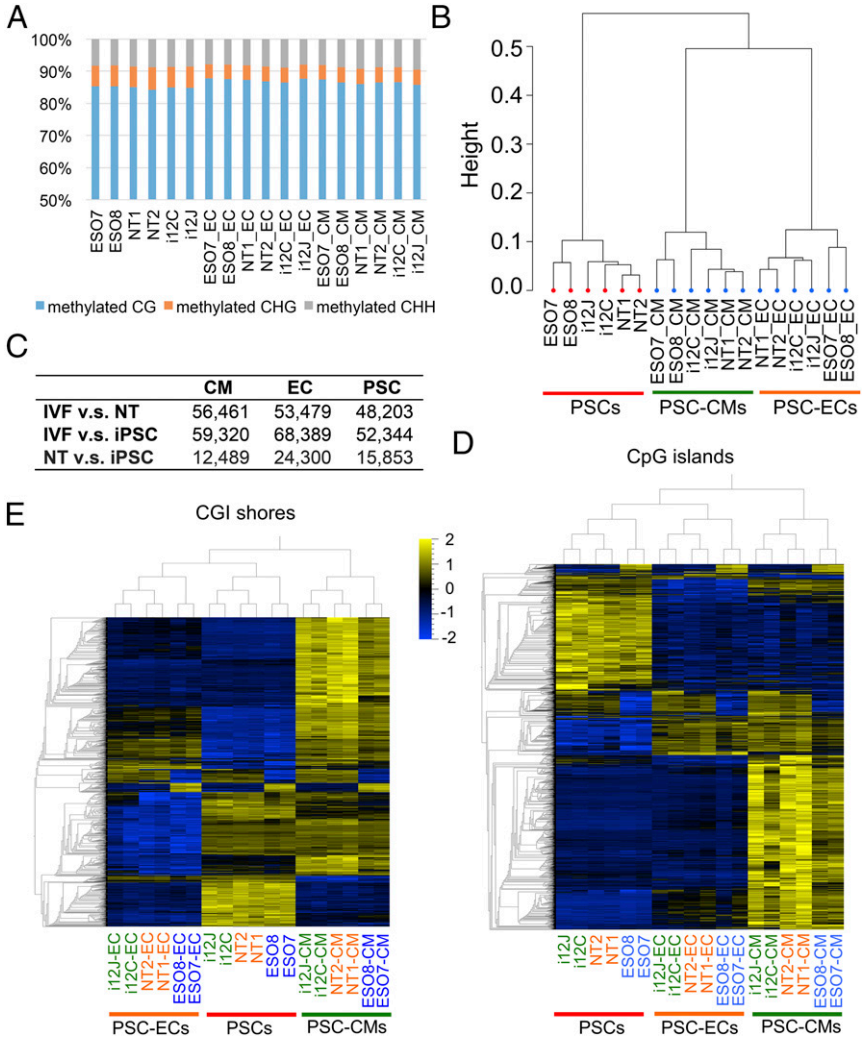

Fig. 4. Global DNA methylome analysis of PSCs, PSC-CMs, and PSC-ECs revealed by RRBS-seq. (*A*) Percentages of mCG, mCHG, and mCHH in all observed 5-methylcytosines in PSCs, PSC-CMs, and PSC-ECs. (*B*) Unsupervised hierarchical clustering of PSCs, PSC-CMs, and PSC-ECs based on global CpG methylation. Each group includes iPSCs (i12C, i12J), nt-ESCs (NT1, NT2), IVF-ESCs (ESO7, ESO8), and their respective differentiated cells (CMs and ECs). The heights of cluster trees reflect the distance (similarity and dissimilarity) among different objects and groups. (*C*) Numbers of DMCs identified using pairwise comparison ($q < 0.01$, methylation difference ≥25%). (*D*) Unsupervised hierarchical clustering of DMRs identified in CGIs across the genome in PSC, PSC-CMs, and PSC-ECs ($q < 0.01$, $n = 3,452$). (*E*) Unsupervised hierarchical clustering of 2,324 CGI-shore DMRs ($q < 0.01$) in PSC, PSC-CMs, and PSC-ECs.

IVF-hypomethylated and IVF-hypermethylated DMRs in CGIs (Fig. 5 *D* and *E*) and promoters (Fig. S8*D*). However, all iPSC-specific DMRs (iDMRs) were hypermethylated in CGIs and promoters, with iPSCs and derivatives displaying significantly higher DNA methylation levels (Fig. 5 *F*–*G*). In contrast, no iDMR was identified in CGI shores, where nt-ESCs and iPSCs exhibited consistent DNA methylation in these conserved DMRs (Fig. 5*B*). Because DNA methylation in promoters is generally correlated with gene expression (23), we then performed Spearman's correlation analysis on these consistent DMRs in CGIs, CGI shores, and promoters. There was a significant negative correlation between promoter DNA methylation and mRNA expression in these conserved DMRs: higher DNA methylation was correlated with lower mRNA expression, whereas lower DNA methylation was associated with higher mRNA abundance (Fig. 5*H*). However, the correlations between DNA methylation and gene expression in CGI and CGI shore consistent DMRs were generally poor (Fig. S8 *E* and *F*). Collectively, these results confirm that the consistent DMRs were primarily associated with the differences between IVF-ESCs and iPSCs, with iPSCs and nt-ESCs sharing fewer DMRs.

In Vitro Assessment of Drug-Induced Toxicity Using Isogenic Human iPSCs and nt-ESCs. One of the most fascinating applications of patient-specific PSCs is personalized drug testing in the dish (12). To assess whether human iPSCs and nt-ESCs are both competent for personalized drug testing, we treated PSC-CMs with doxorubicin, a chemotherapy drug that can lead to cardiomyopathy in some patients. The mechanisms of doxorubicin-induced cardiotoxicity include reactive oxygen species (ROS) formation, programmed cell death (apoptosis), irreversible reductions in ATP production, inhibition of nucleic acid and protein synthesis, and reduced levels of antioxidants (24). To test the dose-dependent effect of doxorubicin on PSC-CMs, we carried out acute (24 h) and long-term (72 h) doxorubicin treatment at four doses: 0.01, 0.1, 1, and 10 μM. Consistent with a previous report (25), all PSC-CMs displayed a dose-dependent response to doxorubicin-induced cardiotoxicity (Fig. S9). For prolonged treatment, PSC-CMs exhibited declines in cell viability and ATP production, and increases in apoptosis, with no significant difference between iPSC-CMs and nt-ESC–CMs at lower doses (Fig. 6 *A*–*C*). We next measured whole-cell hydrogen peroxide (H_2O_2) levels after 24-h treatment when the cell viability was not

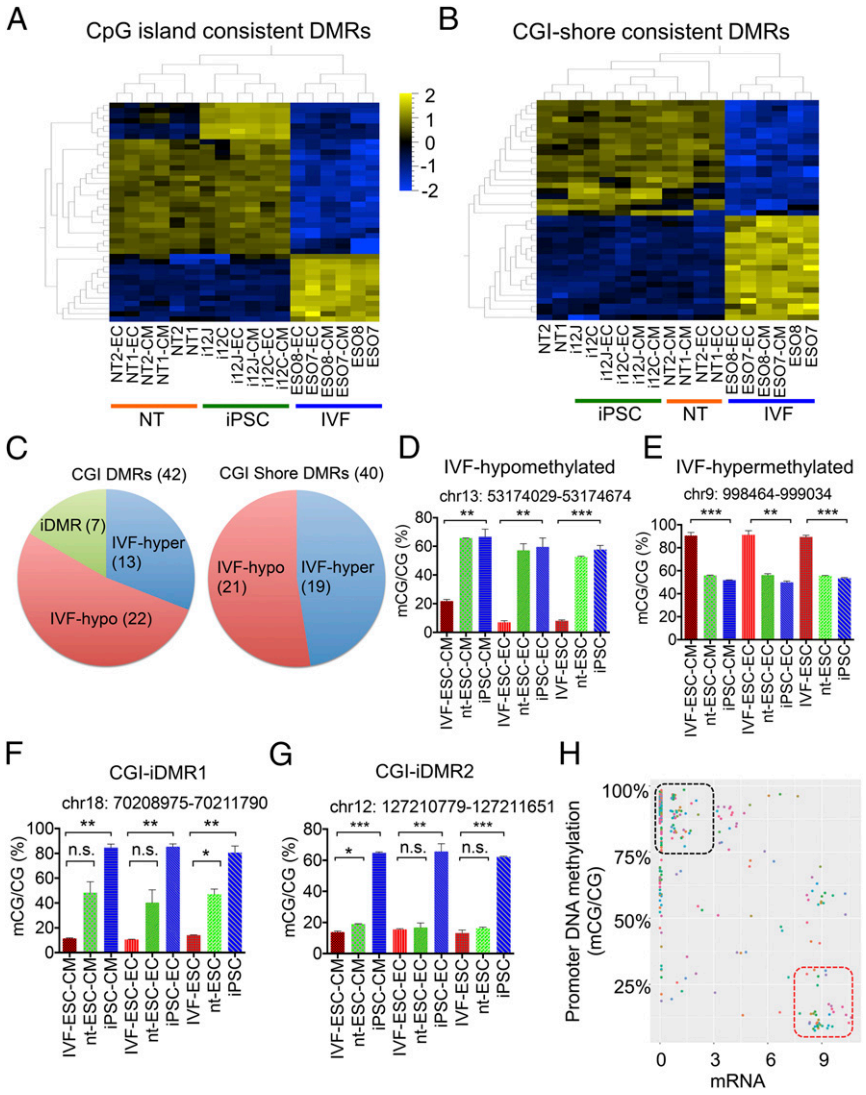

Fig. 5. Consistent CGI and CGI-shore DMRs identified in undifferentiated PSCs and terminally differentiated cells. (*A*) Consistent CGI DMRs ($n = 42$) in PSCs and differentiated cells. (*B*) Consistent CGI-shore DMRs ($n = 40$) were either IVF-hypermethylated or IVF-hypomethylated. (*C*) Numbers of IVF-hypermethylated, IVF-hypomethylated, and iDMRs persistently present in PSCs, PSC-CMs, and PSC-ECs. The iPSC-specific consistent DMRs were not found in CGI-shores. (*D* and *E*) IVF-specific consistent CGI-DMRs identified in undifferentiated PSCs and differentiated cells. (*F* and *G*) Methylation levels of iPSC-specific consistent CGI-DMRs in iPSCs were higher than those in nt-ESCs and IVF-ESCs. (*H*) Spearman's correlation analysis of consistent promoter DMRs and mRNA abundance of the associated genes ($P < 2.2e^{-16}$). All data are represented as mean ± SEM $^*P < 0.05$; $^{**}P < 0.01$; $^{***}P < 0.005$; n.s., not significant; by unpaired two-tailed Student's *t* test and one-way ANOVA.

seriously affected (Fig. 6*D*). ROS levels were dramatically increased upon doxorubicin treatment as low as 0.01 μM (Fig. 6*E*). There were no significant differences in whole-cell ROS generation between iPSC-CMs and nt-ESC–CMs, despite the detection of higher ROS levels in IVF-ESC-CMs. In contrast, the antioxidant glutathione (GSH) was reduced in response to doxorubicin treatment, with higher doses leading to steeper decreases (Fig. 6*F*). Because GSH plays a critical role in the maintenance of mitochondrial function and cell survival, GSH levels can be used as an indicator of oxidative stress in the mitochondria (26). Here we observed a significant difference of GSH levels between iPSC-CMs and nt-ESC–CMs at intermediate doses of doxorubicin (0.1 and 1 μM) (Fig. 6*F*). This was probably due to their distinct sources of mitochondria: iPSC mitochondria came from somatic cells, whereas those of nt-ESCs were inherited from the egg donor, which shared its mitochondria with IVF-ESCs. These results indicate that both iPSC-CMs and nt-ESC–CMs can faithfully recapitulate drug-induced toxicity in a dose-dependent manner, despite divergent origins of mitochondria.

Discussion

In this study, we generated genetically relevant sets of human iPSCs, nt-ESCs, and IVF-ESCs to evaluate the molecular and functional features of differentiated cells derived from these PSCs in vitro. At the cellular level, differentiated cells from isogenic iPSCs and nt-ESCs displayed comparable differentiation efficiency, gene-expression heterogeneity, physiological properties, and metabolic functions. At the transcriptional level, CMs and ECs derived from iPSC were clustered closer to isogenic nt-ESC derivatives than those derived from IVF-ESCs. In addition, genome-wide DNA methylation profiling positioned iPSC-CMs and iPSC-ECs within the same clades of nt-ESC derivatives, which were separated from genetically relevant IVF-ESC descendants. Moreover, both iPSC-CMs and nt-ESC–CMs recapitulated drug-induced cardiotoxicity in a dose-dependent

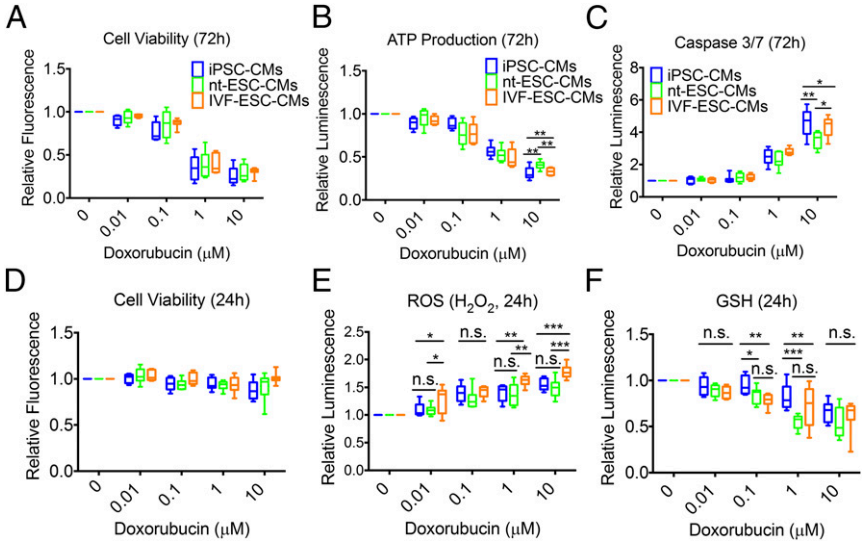

Fig. 6. Doxorubicin-induced toxicity in CMs derived from iPSCs, nt-ESCs, and IVF-ESCs. (*A*) Dose-dependent effect of doxorubicin (72 h) on PSC-CM viability assessed by a Prestoblue cell viability assay ($n = 8$ per group). The relative fluorescence unit was normalized to 0 μM. (*B*) Effect of doxorubicin treatment (72 h) on ATP production of PSC-CMs measured by a CellTiter-Glo assay ($n = 8$ per group). (*C*) Assessment of cellular apoptosis using a luminescent Caspase 3/7 assay after 72-h doxorubicin treatment ($n = 8$ per group). (*D*) Cell viability was not significantly affected in PSC-CMs after 24 h doxorubicin treatment ($n = 8$ per group). (*E*) Whole-cell ROS (H_2O_2) detection in PSC-CMs after administration of doxorubicin (24 h) at four different doses ($n = 8$ per group). (*F*) Acute influence of doxorubicin (24 h) treatment on the mitochondrial GSH concentration assayed by a GSH-Glo Glutathione kit ($n = 8$ per group). All data are represented as mean ± SEM $^*P < 0.05$; $^{**}P < 0.01$; $^{***}P < 0.005$; n.s., not significant; by unpaired two-tailed Student's *t* test and one-way ANOVA.

manner. Therefore, we speculate that terminally differentiated cells derived from different reprogramming mechanisms (iPSC, SCNT, and IVF) are comparable with regard to transcriptomic, epigenomic, cellular, and pharmacological aspects, given that they are genetically identical.

In this study, human iPSCs and nt-ESCs are derived from the same somatic cells (fibroblasts), thus sharing the same nuclear genome. However, their mitochondrial DNA is different due to the maternal inheritance of mitochondria during early embryonic development. In contrast, IVF-ESCs are created using the same egg donor for SCNT; thus, they share the same source of mitochondrial DNA with nt-ESCs, although the nuclear genome of IVF-ESCs is distinct from iPSCs and nt-ESCs. Recent studies indicate that it is important to generate genetically relevant iPSCs, nt-ESCs, and IVF-ESCs to compare their molecular and functional properties, as genetic variation is thought to primarily contribute to the transcriptional heterogeneity among different PSC lines (27–29). Technically, it is extremely challenging to generate these genetically relevant nt-ESCs and IVF-ESCs from the same egg donor due to very limited source of human eggs and ethical concerns. For each superovulation procedure, only 5–15 human eggs can be retrieved from each egg donor (14). The eggs must be further split to derive SCNT and IVF blastocysts, respectively, and subsequently be used for the derivation of nt-ESCs and IVF-ESCs at the same time. Therefore, our study employs unique sets of genetically relevant PSCs generated by different reprogramming mechanisms (SCNT, IVF, and iPSC) and provides a proof-of-concept that differentiated cells derived from isogenic human nt-ESCs and iPSCs are relatively equivalent with respect to molecular, cellular, physiological, and pharmacological features.

At present, patient-specific PSCs can be derived via two approaches: SCNT by enucleated eggs, and iPSC reprogramming by transcription factors. SCNT relies on unknown factors present in the cytoplasm of mature oocytes to remodel the epigenome of somatic cells. These physiological reprogramming factors are developmentally efficient, as they can reprogram somatic cells to a "totipotent" state. The reconstructed embryos by SCNT can survive stringent developmental selection and develop into well-structured blastocysts that are able to produce live cloned offspring, if transferred to proper foster mothers (30). In these aspects, mouse nt-ESCs are developmentally competent and are functionally and transcriptionally indistinguishable from IVF-ESCs (31, 32). Nevertheless, SCNT embryos also carry some developmental defects due to incomplete epigenetic reprogramming, which can be greatly improved using epigenetic modifier (e.g., HDAC inhibitors) in multiple species (pig, sheep, cow, and so forth) (33, 34). In contrast, human iPSC reprogramming has no developmental potential checkpoints, as long as the cells acquire the ability of immortal proliferation (self-renewal) and in vitro pluripotency. Consequently, iPSCs are developmentally and epigenetically compromised in early-passage cells that display epigenetic memory of parental somatic cells and large regions with aberrant DNA methylation patterns, including genomic imprinted domains, which are not seen in nt-ESCs (10, 11, 35). Developmentally, mouse iPSCs can generate viable cloned offspring by tetraploid complementation, although the efficiency is relatively low compared with conventional IVF-ESCs (36). Therefore, we argue that some cells in human iPSC culture may be developmentally compromised, which could not be tested in humans due to ethical constraints. These iPSCs may retain epigenetic memory of somatic cells due to incomplete reprogramming and are unable to generate functional differentiated cells either in vivo or in vitro.

During in vitro differentiation, only authentic PSCs can produce beating CMs and functional endothelial cells in response to specific signaling induction (37). These terminally differentiated cells are essentially the progeny of developmentally competent PSCs residing in the population of iPSCs, nt-ESCs, and IVF-ESCs. Chemically defined culture medium and small-molecule–induced differentiation would reinforce the differentiation of developmentally competent cells within PSCs while eliminating the developmentally incompetent cells (Fig. S10). Thus, the transcriptional and epigenomic characteristics of these terminally differentiated cells are primarily attributed to the genetic compositions rather than the reprogramming methods. In parallel,

genetic make-up is the predominant factor for the transcriptional and epigenomic variations in human iPSCs regardless of their cellular origin (27, 38–41). Although epigenetic memory of somatic cells is potentially present in early-passage iPSCs (6, 10), it is unlikely that functional differentiated cells (CMs and ECs) are derived from iPSCs with substantial somatic cell memory. As proposed in Fig. S10, we hypothesize that terminally differentiated cells derived from iPSCs, nt-ESCs, and IVF-ESCs are comparable with regards to transcriptional, epigenetic, physiological, and pharmacological features, provided that they are genetically identical. Due to the technical and ethical challenges of SCNT and IVF, patient-specific iPSCs will continue to serve as competent in vitro models for human diseases and drug discovery.

Materials and Methods

The protocols and informed consent for human subjects were approved by the Embryonic Stem Cell Research Oversight (SCRO) Committee and the Institutional Review Board (IRB) at Oregon Health & Science University. The experimental designs were also approved by the SCRO and IRB Committees at Stanford University.

Generation of Human iPSC, nt-ESCs, and IVF-ESCs. Human PSCs were maintained in chemically defined E8 medium on Matrigel. The generation of these PSCs is described in details in *SI Materials and Methods*.

Cardiac and Endothelial Differentiation. Cardiac differentiation was induced by a protocol using small chemicals CHIR-99021 and IWR-1. Endothelial differentiation was conducted using CHIR-99021, VEGF, bFGF, and SB431542. Full differentiation protocols are described in *SI Materials and Methods*.

RNA Sequencing. RNA-seq libraries were constructed using an Ion Total RNA-seq Kit v2 (Thermo Fisher Scientific). Deep sequencing was performed in an Ion Proton Sequencer and raw sequencing data were recorded and processed in a local Ion Torrent server. The pipeline for RNA-seq data analysis is described in *SI Materials and Methods*.

RRBS-Seq. RRBS-deq library was prepared using 300 ng of genomic DNA digested with MspI. NEBNext Index Primers were used to barcode different samples. Six barcoded RRBS-seq libraries were pooled together and loaded to an Illumina HiSeq 4000 for deep sequencing. Raw data were processed using BS-Seeker 2.0 and DNA methylation calling was performed using MethylKit package (detailed in *SI Materials and Methods*).

ACKNOWLEDGMENTS. We thank Caressa Chen for helping with Ion Torrent sequencing; Yingxin Li for electrophysiological analysis; and Larry Bowen and Blake Wu for critical editing of this manuscript. Reduced-representation bisulfite sequencing was performed at the Genome Sequencing Service Center by Stanford Center for Genomics and Personalized Medicine, supported by NIH Grant S10OD020141. This study was supported by NIH Grants R01 HL113006, R01 HL126527, R01 HL123968, and R01 HL130020 (to J.C.W.), R24 HL117756 (to J.C.W. and M.P.S.), and P01 GM099130 (to M.P.S.); and California Institute for Regenerative Medicine (CIRM) Grant GC1R-06673-A (to M.P.S.) and CIRM Grant RT3-07798 (to J.C.W.); and AHA Grants 17MERIT33610009 (to J.C.W.) and 17IRG33410532 (to I.K.). Studies in the laboratory of S.M. were supported by the Leducq Foundation and OHSU Institutional funds. M.-T.Z. and Q.L. were partially supported by research awards from the Lucile Packard Foundation for Children's Health, Stanford NIH-National Center for Advancing Translational Sciences-Clinical Translational Science Award UL1 TR001085, and the Child Health Research Institute of Stanford University.

1. Yamanaka S, Blau HM (2010) Nuclear reprogramming to a pluripotent state by three approaches. *Nature* 465:704–712.
2. Yang X, et al. (2007) Nuclear reprogramming of cloned embryos and its implications for therapeutic cloning. *Nat Genet* 39:295–302.
3. Jaenisch R (2004) Human cloning—The science and ethics of nuclear transplantation. *N Engl J Med* 351:2787–2791.
4. Thomson JA, et al. (1998) Embryonic stem cell lines derived from human blastocysts. *Science* 282:1145–1147.
5. Choi J, et al. (2015) A comparison of genetically matched cell lines reveals the equivalence of human iPSCs and ESCs. *Nat Biotechnol* 33:1173–1181.
6. Hu S, et al. (2016) Effects of cellular origin on differentiation of human induced pluripotent stem cell-derived endothelial cells. *JCI Insight* 1:e85558.
7. Kim K, et al. (2011) Donor cell type can influence the epigenome and differentiation potential of human induced pluripotent stem cells. *Nat Biotechnol* 29:1117–1119.
8. Lister R, et al. (2011) Hotspots of aberrant epigenomic reprogramming in human induced pluripotent stem cells. *Nature* 471:68–73.
9. Johannesson B, et al. (2014) Comparable frequencies of coding mutations and loss of imprinting in human pluripotent cells derived by nuclear transfer and defined factors. *Cell Stem Cell* 15:634–642.
10. Kim K, et al. (2010) Epigenetic memory in induced pluripotent stem cells. *Nature* 467: 285–290.
11. Ma H, et al. (2014) Abnormalities in human pluripotent cells due to reprogramming mechanisms. *Nature* 511:177–183.
12. Avior Y, Sagi I, Benvenisty N (2016) Pluripotent stem cells in disease modelling and drug discovery. *Nat Rev Mol Cell Biol* 17:170–182.
13. Chen IY, Matsa E, Wu JC (2016) Induced pluripotent stem cells: At the heart of cardiovascular precision medicine. *Nat Rev Cardiol* 13:333–349.
14. Tachibana M, et al. (2013) Human embryonic stem cells derived by somatic cell nuclear transfer. *Cell* 153:1228–1238.
15. Fearnley CJ, Roderick HL, Bootman MD (2011) Calcium signaling in cardiac myocytes. *Cold Spring Harb Perspect Biol* 3:a004242.
16. Melé M, et al.; GTEx Consortium (2015) Human genomics. The human transcriptome across tissues and individuals. *Science* 348:660–665.
17. Hara N, et al. (2007) Elevation of cellular NAD levels by nicotinic acid and involvement of nicotinic acid phosphoribosyltransferase in human cells. *J Biol Chem* 282:24574–24582.
18. Stojanovski D, Koutsopoulos OS, Okamoto K, Ryan MT (2004) Levels of human Fis1 at the mitochondrial outer membrane regulate mitochondrial morphology. *J Cell Sci* 117:1201–1210.
19. Nishizawa M, et al. (2016) Epigenetic variation between human induced pluripotent stem cell lines is an indicator of differentiation capacity. *Cell Stem Cell* 19:341–354.
20. Schübeler D (2015) Function and information content of DNA methylation. *Nature* 517:321–326.
21. Meissner A, et al. (2008) Genome-scale DNA methylation maps of pluripotent and differentiated cells. *Nature* 454:766–770.
22. Deaton AM, Bird A (2011) CpG islands and the regulation of transcription. *Genes Dev* 25:1010–1022.
23. Jones PA (2012) Functions of DNA methylation: Islands, start sites, gene bodies and beyond. *Nat Rev Genet* 13:484–492.
24. Takemura G, Fujiwara H (2007) Doxorubicin-induced cardiomyopathy from the cardiotoxic mechanisms to management. *Prog Cardiovasc Dis* 49:330–352.
25. Burridge PW, et al. (2016) Human induced pluripotent stem cell-derived cardiomyocytes recapitulate the predilection of breast cancer patients to doxorubicin-induced cardiotoxicity. *Nat Med* 22:547–556.
26. Marí M, Morales A, Colell A, García-Ruiz C, Fernández-Checa JC (2009) Mitochondrial glutathione, a key survival antioxidant. *Antioxid Redox Signal* 11:2685–2700.
27. Rouhani F, et al. (2014) Genetic background drives transcriptional variation in human induced pluripotent stem cells. *PLoS Genet* 10:e1004432.
28. Kilpinen H, et al. (2017) Common genetic variation drives molecular heterogeneity in human iPSCs. *Nature* 546:370–375.
29. Zhao MT, et al. (2017) Cell type-specific chromatin signatures underline regulatory DNA elements in human induced pluripotent stem cells and somatic cells. *Circ Res* 121: 1237–1250.
30. Wilmut I, et al. (2002) Somatic cell nuclear transfer. *Nature* 419:583–586.
31. Wakayama S, et al. (2006) Equivalency of nuclear transfer-derived embryonic stem cells to those derived from fertilized mouse blastocysts. *Stem Cells* 24:2023–2033.
32. Brambrink T, Hochedlinger K, Bell G, Jaenisch R (2006) ES cells derived from cloned and fertilized blastocysts are transcriptionally and functionally indistinguishable. *Proc Natl Acad Sci USA* 103:933–938.
33. Keefer CL (2015) Artificial cloning of domestic animals. *Proc Natl Acad Sci USA* 112: 8874–8878.
34. Mao J, et al. (2015) Oxamflatin treatment enhances cloned porcine embryo development and nuclear reprogramming. *Cell Reprogram* 17:28–40.
35. Stadtfeld M, et al. (2010) Aberrant silencing of imprinted genes on chromosome 12qF1 in mouse induced pluripotent stem cells. *Nature* 465:175–181.
36. Zhao XY, et al. (2009) iPS cells produce viable mice through tetraploid complementation. *Nature* 461:86–90.
37. Burridge PW, Keller G, Gold JD, Wu JC (2012) Production of de novo cardiomyocytes: Human pluripotent stem cell differentiation and direct reprogramming. *Cell Stem Cell* 10:16–28.
38. Burrows CK, et al. (2016) Genetic variation, not cell type of origin, underlies the majority of identifiable regulatory differences in iPSCs. *PLoS Genet* 12:e1005793.
39. Krijger PH, et al. (2016) Cell-of-origin-specific 3D genome structure acquired during somatic cell reprogramming. *Cell Stem Cell* 18:597–610.
40. Kyttälä A, et al. (2016) Genetic variability overrides the impact of parental cell type and determines iPSC differentiation potential. *Stem Cell Reports* 6:200–212.
41. Ghosh Z, et al. (2010) Persistent donor cell gene expression among human induced pluripotent stem cells contributes to differences with human embryonic stem cells. *PLoS One* 5:e8975.